Hindawi
Geofluids
Volume 2021, Article ID 3095690, 13 pages
https://doi.org/10.1155/2021/3095690

Research Article

An Analysis of the Impact of Deviatoric Stress and Spherical Stress on the Stability of Surrounding Rocks in Roadway

Liu Rui[1] **and Zhu Quanjie**[2]

[1]*School of Energy and Mining Engineering, China University of Mining and Technology (Beijing), 100083 Beijing, China*
[2]*School of Emergency Technology and Management, North China Institute of Science and Technology, Beijing 101601, China*

Correspondence should be addressed to Liu Rui; bukaopu999@gmail.com

Received 27 June 2021; Accepted 5 August 2021; Published 31 August 2021

Academic Editor: Hualei Zhang

In this study, a detailed analysis was conducted to evaluate the impacts of the deviatoric stress component and spherical stress component on the stability of surrounding rocks in the roadway via the theoretical analysis and calculation and numerical simulation. Based on the analysis, the distribution laws guiding the main stress differences, plastic zone, convergence of surrounding rocks, and third invariant of stress under various conditions (such as equal spherical stress and unequal deviatoric stress and equal deviatoric stress and unequal spherical stress) were developed, providing an optimization scheme for roadway support misunderstanding under the conditions of high spherical stress field and high deviator stress field. The study further reveals that under the circumstance of the constant spherical stress, the greater the deviatoric stress, the plastic zone range of the surrounding rock of the roadway, the range of tensile deformation of the surrounding rock, the amount of convergence of the surrounding rock, the probability of separation of the roof and floor of the roadway, and the principal stress difference and the main stress, the greater the concentration range of the maximum stress difference is, and the maximum principal stress difference is mainly concentrated in the roof and floor rocks of the roadway, and the greater the deviatoric stress, the greater the probability that the roof and floor rocks of the roadway will be separated, and the maximum principal stress difference is mainly concentrated in the roof and floor rocks of the roadway, the greater the deviator stress, the greater the concentration range of the maximum value of the principal stress difference and the principal stress difference; when the deviator stress is constant, the range of the plastic zone and the maximum principal stress difference concentration range of the surrounding rock of the roadway decrease with the increase of the ball stress, and the principal stress difference, the amount of convergence of the surrounding rock, and the range of tensile deformation increase with the increase of the ball stress. The maximum principal stress difference is mainly concentrated in the roof and floor rocks of the roadway. The principal stress difference increases with the increase of the spherical stress, and the maximum concentration range of the principal stress difference decreases with the increase of the spherical stress. After the method proposed in this paper optimizes the actual roadway support on site, the surrounding rock deformation of the roadway is small and the control is relatively ideal, which basically meets the engineering needs.

1. Introduction

Ground stress has been considered as the fundamental force causing deformations and damages in various underground excavation projects [1, 2] and one of the important bases for designing the support and protection system of the underground projects. Ground stress has been divided into two categories including self-weight stress and horizontal tectonic stress. Therefore, scholars domestically and abroad have invested substantial time and energy in researching the impacts of self-weight stress [3–6] and horizontal tectonic stress [7–10] on the stability of the roadway surrounding rocks.

Based on plastic mechanics, the stress of surrounding rocks can be categorized into spherical stress tensor and deviatoric stress tensor, with the former one deciding the shape changes of the rocks and the latter one dominating the volume changes [11]. Substantial studies have been

conducted to explore the distribution laws of spherical stress of roadway surrounding rocks and plastic zone. Ma et al. researched the deviatoric stress field and the distribution law of plastic zone when the roadway surrounding rocks are exposed to uneven stresses [12]. Yu et al. investigated the impacts of deviatoric stress on the plastic zone distribution of roadway surrounding rocks, resulting in the identification of an instability model of the roadway under various lateral pressure coefficients [13]. Xie et al. studied the variance law of deviatoric stress of deep roadway surrounding rocks and proposed asymmetric control technology of surrounding rocks based on various sections [14]. He et al. focused their studies on the structural stress of deep roadway surrounding rocks at high elevation including the damage and the distribution of deviatoric stress, along with corresponding controlling measures [15]. Xu et al. took the superelevation section of a coal mine track in Shanxi as the research object, used UDEC to simulate the deviatoric stress distribution of the surrounding rock of the roadway at different roadway heights, compared the degree of deviatoric stress changes between the roof and floor and the two sides of the roadway, and finally proposed targeted support technology [16]. Luo et al. thoroughly studied the influence of the intermediate principal stress and the rheological properties of the surrounding rock on the displacement of the surrounding rock of the roadway and the plastic zone of the surrounding rock and finally found that ignoring the rheological properties of the rock would overestimate the lithology of the surrounding rock. In control roadway deformation and plastic zone expansion [17], Zhang et al. used the D-P yield criterion to calculate the analytical solutions for the elastoplasticity, plastic zone radius, and displacement of the surrounding rock under bidirectional isobaric conditions and discovered the importance of the intermediate principal stress to the stress distribution of the surrounding rock [18]. According to the D-P yield criterion and the nonassociated flow rule, Chen et al. derived a closed analytical solution for the stress, deformation, and radius of the plastic zone of the surrounding rock of a deep circular roadway under hydrostatic pressure [19].

Scholars have conducted sufficient studies on the deviatoric stress distribution of roadway surrounding rocks and the distribution law of the plastic zone after the roadway excavation. However, limited studies have been performed on the impacts of both spherical stress tensor and deviatoric stress tensor before the roadway excavation on the roadway stability after excavation. Therefore, in this study, a detailed analysis was conducted to evaluate the impacts of deviatoric stress component and spherical stress component on the stability of surrounding rocks in roadway via the theoretical analysis and calculation, numerical simulation, and two sets of loading tests.

2. Loading Plan and Numerical Model

2.1. Loading Plan and the Analysis of Principal Stress Difference of Roadway Surrounding Rock. A plan including two sets of loading tests was proposed to study the impacts of the deviatoric stress component and spherical stress component on the stability of surrounding rocks in the roadway. The detailed loading plan is provided below.

A loading test was performed at a constant spherical stress component ($p = 15$ MPa) and various deviatoric stress components ($q = 2.4$ MPa, 7.2 MPa, 12 MPa, and 16.8 MPa). In other words, during this loading test, constant spherical stress was imposed on the model with different deviatoric stresses.

A loading test was performed at a constant deviatoric stress component ($q = 12$ MPa) and various spherical stress components ($p = 9$ MPa, 12 MPa, 15 MPa, and 18 MPa). In other words, during this loading test, constant deviatoric stress was imposed on the model with different spherical stresses.

$$p = \frac{1}{3}(\sigma_1 + \sigma_2 + \sigma_3), \tag{1}$$

$$q = \frac{1}{\sqrt{2}}\sqrt{(\sigma_1 - \sigma_2)^2 + (\sigma_2 - \sigma_3)^2 + (\sigma_3 - \sigma_1)^2}. \tag{2}$$

Equation (3) can be obtained based on equations (1) and (2) listed above.

$$\begin{Bmatrix} \sigma_1 \\ \sigma_2 \\ \sigma_3 \end{Bmatrix} = \begin{Bmatrix} p \\ p \\ p \end{Bmatrix} + \frac{2}{3}q \begin{Bmatrix} \sin\left(\theta_\sigma + \frac{2}{3}\pi\right) \\ \sin\theta_\sigma \\ \sin\left(\theta_\sigma - \frac{2}{3}\pi\right) \end{Bmatrix}, \tag{3}$$

where p refers to spherical stress, q indicates deviatoric stress, and θ_σ is the loading angle.

A stress space diagram was obtained from equation (3) and illustrated in Figure 1.

The strain increment of the deep surrounding rocks under the plastic strain state demonstrated pure shear deformation with the maximum shear stress dominating the generation of the stratum plastic zone and development [20, 21]. The principal stress difference can reflect the shear stress distribution and the damage in the surrounding rocks [22, 23]. The principal stress difference can be illustrated in

$$\sigma_s = \sigma_1 - \sigma_3. \tag{4}$$

Based on the elasticity theory, the stress of the circular hole in the two-way stress infinite plate is shown in

$$\begin{cases} \sigma_r = \frac{1}{2}(\sigma_v + \sigma_H)\left(1 - \frac{R_0^2}{r^2}\right) - \frac{1}{2}(\sigma_v - \sigma_H)\left(1 - 4\frac{R_0^2}{r^2} + 3\frac{R_0^4}{r^4}\right)\cos 2\theta, \\ \sigma_\theta = \frac{1}{2}(\sigma_v + \sigma_H)\left(1 + \frac{R_0^2}{r^2}\right) + \frac{1}{2}(\sigma_v - \sigma_H)\left(1 + 3\frac{R_0^4}{r^4}\right)\cos 2\theta, \\ \tau_{r\theta} = \frac{1}{2}(\sigma_H - \sigma_v)\left(1 + 2\frac{R_0^2}{r^2} - 3\frac{R_0^4}{r^4}\right)\sin 2\theta, \end{cases} \tag{5}$$

where σ_v refers to the vertical stress in MPa, σ_H indicates

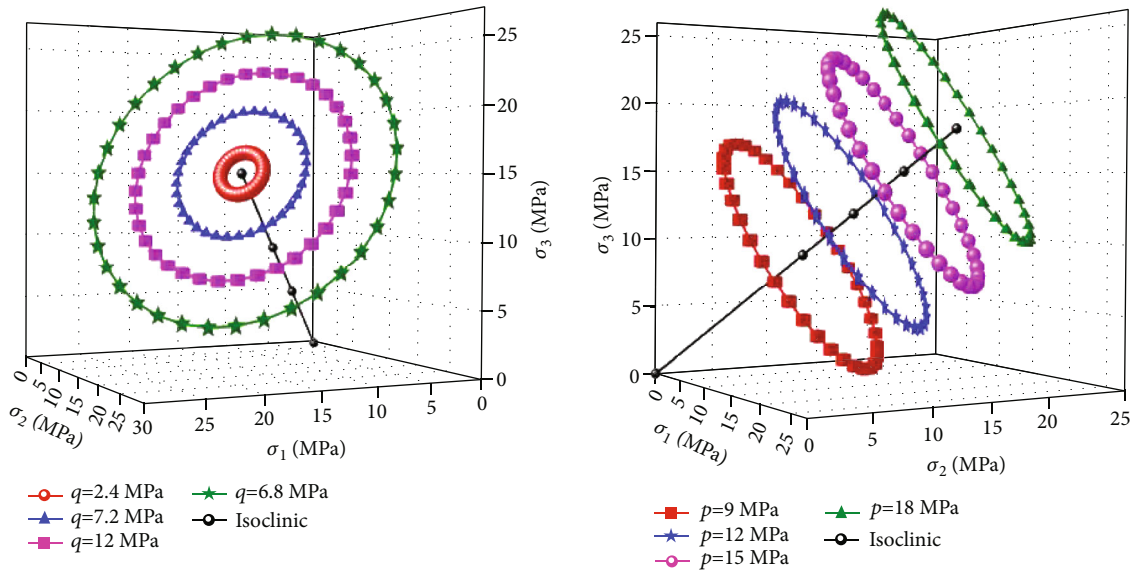

(a) The stress space diagram under the constant deviatoric stress (b) The stress space diagram under the constant spherical stress

Figure 1: The distribution of stress and space.

the horizontal stress in MPa, R_0 is the radius of the circular hole in m, and θ represents the polar angle.

Under the state of the plane strain, the principal stress can be calculated following

$$\sigma_1 = \frac{\sigma_x + \sigma_y}{2} + \sqrt{\left(\frac{\sigma_x + \sigma_y}{2}\right)^2 + \tau_{xy}^2}, \tag{6}$$

$$\sigma_3 = \frac{\sigma_x + \sigma_y}{2} - \sqrt{\left(\frac{\sigma_x + \sigma_y}{2}\right)^2 + \tau_{xy}^2}, \tag{7}$$

where σ_1 refers to the maximum principal stress in MPa and σ_3 indicates the minimum principal stress in MPa. Equations (6) and (7) can be converted into equations (8) and (9) under polar coordinates.

$$\sigma_1 = \frac{1}{2}(\sigma_r + \sigma_\theta) + \frac{1}{2}\sqrt{(\sigma_r - \sigma_\theta)^2 + 4\tau_{r\theta}^2}, \tag{8}$$

$$\sigma_3 = \frac{1}{2}(\sigma_r + \sigma_\theta) - \frac{1}{2}\sqrt{(\sigma_r - \sigma_\theta)^2 + 4\tau_{r\theta}^2}. \tag{9}$$

Considering the roadway as the plane strain allows the overlook of the principal stress, based on equations (3) and (5), equation (10) can be obtained.

$$\begin{Bmatrix} \sigma_H \\ \sigma_v \end{Bmatrix} = \begin{Bmatrix} p \\ p \end{Bmatrix} + \frac{2}{3}q \begin{Bmatrix} \sin\left(\theta_\sigma + \frac{2}{3}\pi\right) \\ \sin\left(\theta_\sigma - \frac{2}{3}\pi\right) \end{Bmatrix}. \tag{10}$$

Under various deviatoric stresses, -10° load was selected for load while -20° load was selected under various spherical stresses. Based on equation (4) to equation (10), the surrounding principal stress differences of the circular hole under various conditions were obtained and presented in Figure 2.

Based on Figure 2, the following results can be obtained. (1) Under constant spherical stress, as the deviatoric stress increases, the principal stress difference on the vertical direction tends to increase accordingly, with the principal stress difference of shallow surrounding rocks greater than that of deep surrounding rocks. Horizontally, the principal stress difference of shallow surrounding rocks decreases as the deviatoric stress increases while the principal stress difference of deep surrounding rocks increases. Overall, the vertical principal stress difference is greater than the horizontal one. (2) Under constant deviatoric stress, as the spherical stress increases, the vertical principal stress difference increases, with the principal stress difference of shallow surrounding rocks greater than that of deep surrounding rocks. Horizontally, the principal stress difference of shallow surrounding rocks increases as the spherical stress increases while the principal stress difference of deep surrounding rocks decreases. Overall, the vertical principal stress difference is greater than the horizontal one.

2.2. Numerical Model and Parameters. A numerical simulation was performed to analyze the impacts of deviatoric stress and spherical stress on the stability of surrounding rocks in the roadway. In the simulation model, the cross section of the roadway was designed in a semicircular arch, with a height of 3500 mm and a width of 4000 mm. The calculation range was set at 50 m × 50 m. The sides and the bottom of the model limited the horizontal and vertical displacements. The rock mass mechanical parameters of each rock stratum are shown in Table 1. Stresses were loaded to the model following the loading plan listed in Section 2.1.

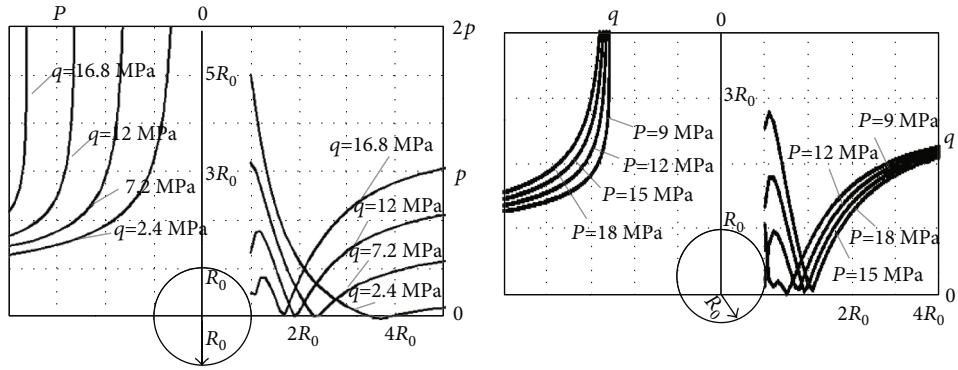

(a) The surrounding principal stress differences of the circular hole under a constant deviatoric stress

(b) The surrounding principal stress differences of the circular hole under a constant spherical stress

Figure 2: The distribution of principal stress difference around circular hole.

Table 1: The rock mass mechanical parameters.

Rock formation	ρ (kg·cm^{-3})	K (GPa)	G (GPa)	Cohesion (MPa)	R_m (MPa)	α (°)
Upper rock mass	2600	8.82	4.63	4.0	2.6	34
Limestone	2800	5.57	4.53	8.4	4.7	38
Argillaceous siltstone	2570	13.4	7.5	2.5	1.8	32
Medium sandstone	2580	3.3	2.5	1.6	1.3	25
Siltstone	2620	7.52	3.1	1.9	1.2	26
Sand shale	2660	5.7	3.4	1.8	1.7	26
Sandy mudstone	2500	3.68	2.15	1.5	1.12	28
Lower rock mass	2695	5.2	4.1	3.3	2.12	35

3. The Test Results under a Constant Spherical Stress

3.1. The Distribution Law of the Principal Stress Difference of the Roadway Surrounding Rocks. With FLAC^{3D}, a cloud diagram shown in Figure 3 was drafted to demonstrate the principal stress difference of the roadway surrounding rocks under constant spherical stress and various deviatoric stresses.

From Figure 3, the following results can be obtained. (1) When $q = 2.4$ MPa, the maximum principal stress difference concentrated within 2 to 5 m range of the roadway surrounding rocks, with maximum principal stress difference observed in the lower stratum of the surrounding rocks. As the deviatoric stress increased, the maximum principal stress difference continued to increase, which is consistent with the trend demonstrated in Figure 2(a), suggesting a higher shear resistance needed in the anchor bolt (cable) installed in the roadway roof in a high deviatoric stress field. (2) As the deviatoric stress increased, the concentration zone of the maximum principal stress in the roadway surrounding rock continued to expand and migrate to the deep layers of rocks, which suggests that longer anchor cables are needed to keep anchor cables fixed to the roof for the purpose of support protection. (3) The deviatoric stress had limited impacts on the principal stress difference of the roadway sides.

3.2. The Variance Law of the Plastic Zone of the Roadway Surrounding Rocks. The distribution of the plastic zone contributes to the identification of the supported depth. The distribution of plastic zone under various deviatoric stresses is demonstrated in Figure 4. The damage depth of the surrounding rock corresponding to the deviatoric stress is shown in Figure 5.

Based on Figures 4 and 5, the following results can be drawn. (1) As the deviatoric stress increases, the plastic zone in the roadway roof grows large, suggesting that longer supporting plates are needed to enhance the stability of the roadway in a high deviatoric stress field, which is consistent with Figure 3. (2) When $q < 16.8$ MPa, the increase of deviatoric stress tends to have limited impacts on the damage of roadway sides. When $q = 16.8$ MPa, the damage of roadway sides increases drastically. Taking Figure 3 into consideration, the maximum principal stress difference concentrates in the lower stratum of the roadway roof. In addition, higher deviatoric stress leads to a larger maximum principal stress difference concentration zone. Therefore, the expansion of the maximum principal stress difference concentration zone is the main cause of the drastic increases in the damage of roadway sides, indicating that proper support and protection are critical to prevent the roadway instability caused by the damage of roadway sides under high deviatoric stress.

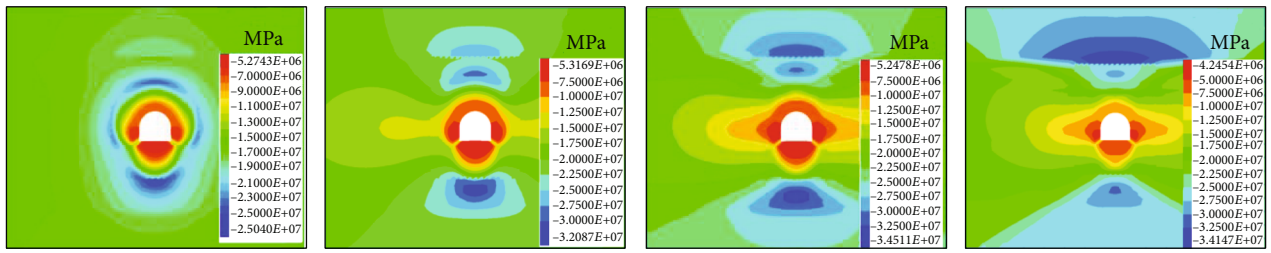

Figure 3: The principal stress difference under different deviatoric stresses.

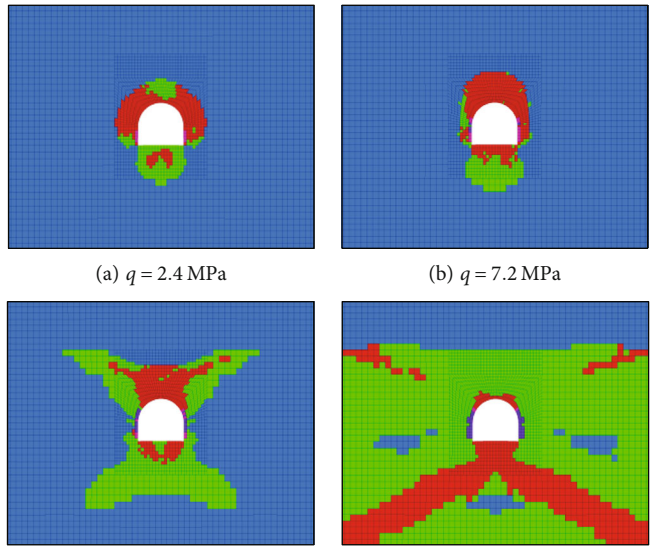

(a) $q = 2.4$ MPa (b) $q = 7.2$ MPa

(c) $q = 12$ MPa (d) $q = 16.8$ MPa

Figure 4: The distribution of plastic zone under various deviatoric stresses. Blue is no damage, red is raw shear failure, and green is shear failure has occurred.

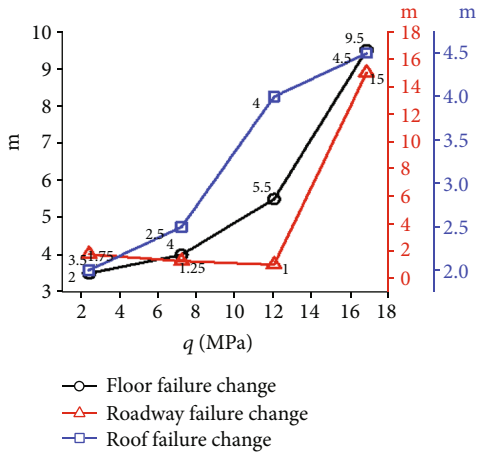

Figure 5: The damage depth of the surrounding rocks corresponding to the deviatoric stress.

3.3. The Deformation Law of the Surrounding Rocks. The deformation degree of the surrounding rocks can reflect the need for ductility of the support system. Under various deviatoric stresses, the deformation of the roadway surrounding rocks from the surface to the depth is demonstrated in Figure 6.

According to Figure 6, (1) the displacement of surrounding rock from shallow to deep decreases in a "logarithmic" pattern, until reaching stability. (2) When $q > 7.2$ MPa, negative displacement was observed at the 3 m of roadway floor in-depth and 2 m of roadway roof, which suggests that in the floor, the deep rock stratum submerges while the shallow ones rise. On the other hand, the deep rock stratum rises while the shallow ones submerge in the roof. The observations suggest that higher deviatoric stress tends to increase the probability of separation in the roadway roof and floor, resulting in a higher possibility of roof collapse and bottom drum. (3) The surface displacement of the roadway can reflect the maximum deformation of the roadway surrounding rocks, the damage of the shallow surrounding rocks, and separation. According to Figure 6, as the deviatoric stress increases, the surface displacement of the roadway increases in a linear pattern. When q increased above 2 MPa, the surface displacement of the roadway decreases, which suggests that when q is higher than 12 MPa, the deep stratum in the roadway roof starts to rise substantially, resulting in a reduced convergence of the surrounding rocks.

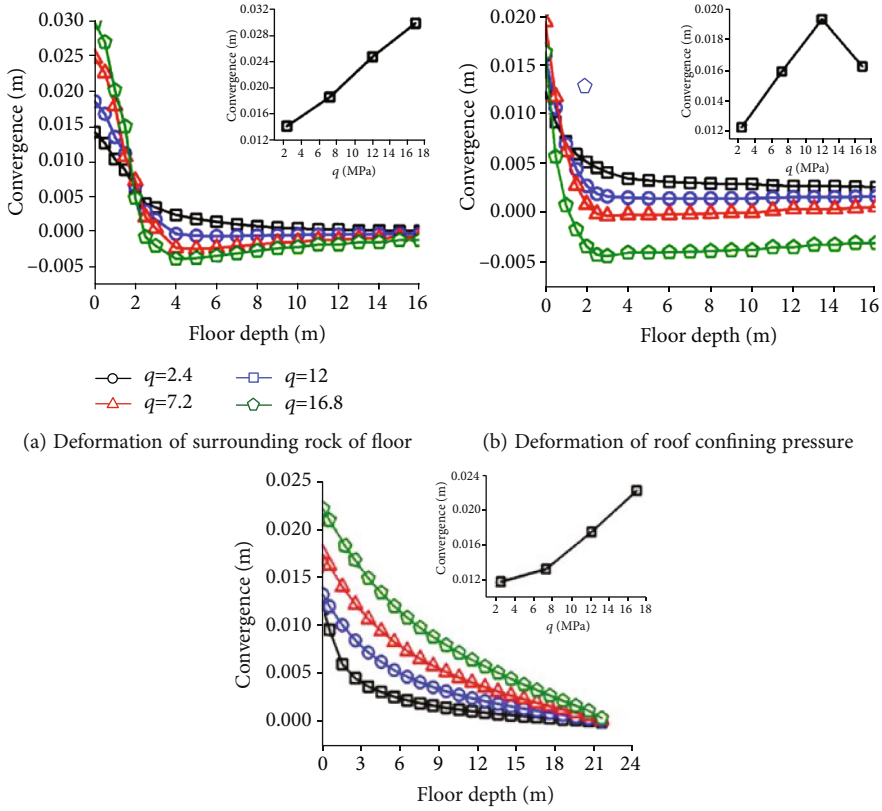

(a) Deformation of surrounding rock of floor

(b) Deformation of roof confining pressure

(c) Deformation of surrounding rock of roadside

Figure 6: The convergence of surrounding rocks under various deviatoric stresses.

3.4. The Distribution Law of the Third Invariant of Deviatoric Stress in Surrounding Rocks. The third invariant of deviatoric stress J_3 can be used to identify the deformation type of the surrounding rocks. When $J_3 < 0$, the deformation is categorized as compressive deformation. When $J_3 = 0$, the deformation is considered as planar deformation. When $J_3 > 0$, the deformation is rated as tensile deformation [8]. The third invariant of deviatoric stress J_3 can be a comprehensive index of combining the maximum principal stress, minimum principal stress, and medium principal stress, indicating the deformation type of the surrounding rocks. The third invariant of deviatoric stress J_3 can be expressed in

$$J_3 = \left(\frac{2\sigma_1 - \sigma_2 - \sigma_3}{3}\right)\left(\frac{2\sigma_2 - \sigma_3 - \sigma_1}{3}\right)\left(\frac{2\sigma_3 - \sigma_1 - \sigma_2}{3}\right). \tag{11}$$

A cloud diagram shown in Figure 7 was obtained to demonstrate the third invariant under various deviatoric stresses. According to Figure 7, when $q = 2.4$ MPa, a tensile stress zone was observed within 0.3 to 2.5 m range of the roadway surrounding rocks. As the deviatoric stress increases, the tensile stress zone expands, resulting in a larger tensile stress concentration zone in roadway sides and bottom than the roof. Due to the poor tensile strength of the rocks, high tensile stress can jeopardize the stability of the roadway surrounding rocks. Therefore, a high pretorque value should be adopted to the supporting system of the roadway surrounding rocks in a high deviatoric stress field to enhance the load capacity of the surrounding the rocks in roadway.

4. The Test Results under a Constant Deviatoric Stress

4.1. The Distribution Law of the Principal Stress Difference of the Roadway Surrounding Rocks. A cloud diagram shown in Figure 8 was drafted to demonstrate the principal stress difference of the roadway surrounding rocks under constant deviatoric stress and various spherical stresses.

According to Figure 8, (1) as the spherical stress increases, the maximum principal stress concentration range in the deep surrounding rocks tends to decrease, suggesting that in a high spherical stress field, the layout and installation of the anchor bolts and cables should avoid the principal stress concentration zone for better supporting and stability. (2) As the spherical stress increases, the principal stress difference increases in the surrounding rocks of the roadway bottom, which is consistent with Figure 2(b), demanding a higher shear resistance in the anchor bolts and cables. (3) The spherical stress exerts some influences on the principal stress difference of the shallow surrounding rocks in the roadway sides. However, such influence is limited to the deep surrounding rocks, which is also

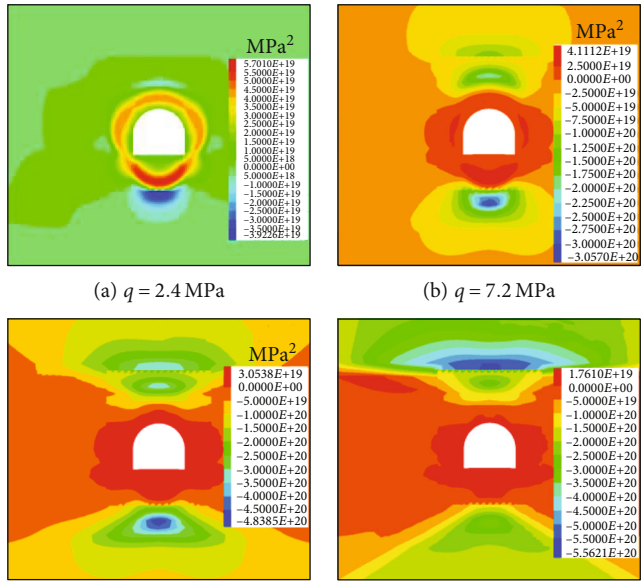

(a) $q = 2.4$ MPa (b) $q = 7.2$ MPa

(c) $q = 12$ MPa (d) $q = 16.8$ MPa

Figure 7: The J_3 distribution under various deviatoric stresses.

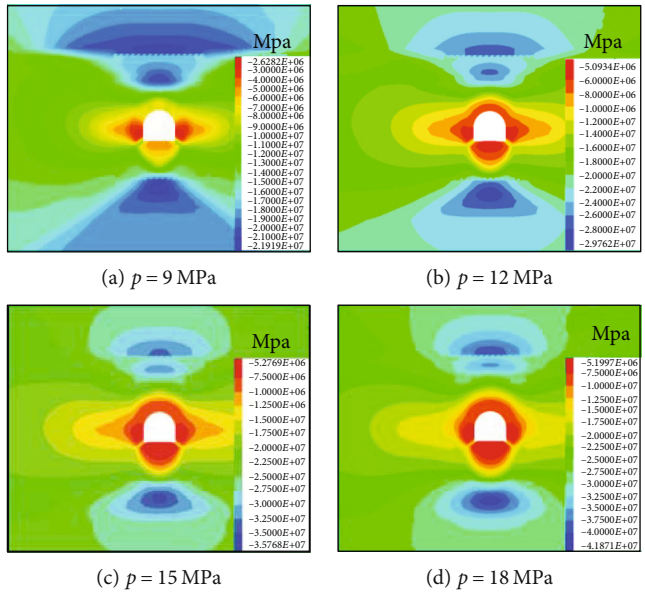

(a) $p = 9$ MPa (b) $p = 12$ MPa

(c) $p = 15$ MPa (d) $p = 18$ MPa

Figure 8: Principal stress difference of the surrounding rocks.

demonstrated in Figure 2(b), resulting in a lower shear resistance requirement to the supporting and protection system of the roadway sides.

4.2. The Deformation Law of the Surrounding Rocks. The distribution of plastic zone under various spherical stresses is demonstrated in Figure 9. The damage depth of the surrounding rock corresponding to the spherical stress is shown in Figure 10.

According to Figures 9 and 10, (1) as the spherical stress increases, the plastic zone of the roadway surrounding rocks tends to decrease due to the increased surrounding pressure on the roadway surrounding rocks under higher spherical stress. In other words, a higher surrounding pressure leads to a higher strength of the surrounding rock and a smaller plastic zone. (2) Under various spherical stresses, the plastic zone of the roadway surrounding rock demonstrates a butterfly shape. The spherical stress only impacts the range of the plastic zone instead of the shape. Comparing with Figure 5 has revealed that the deviatoric stress tends to exert a greater impact on the surrounding rocks of the roadway. (3) The damage depth of the roadway surrounding rocks demonstrates a higher sensitivity to the spherical stress while the damage of the roadway sides is less sensitive.

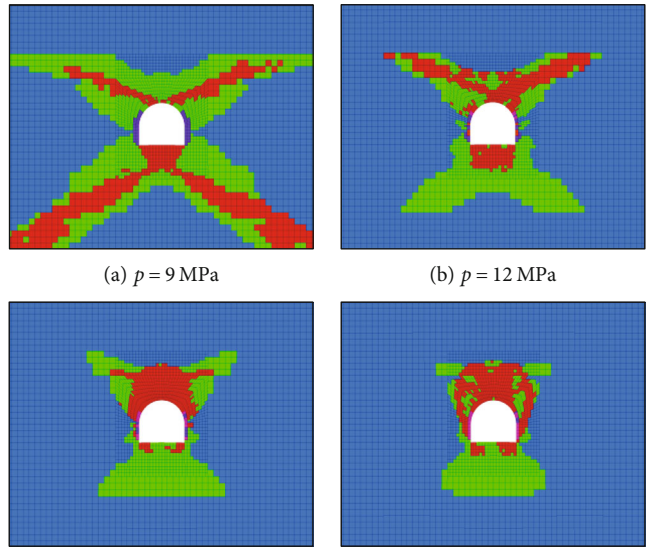

(a) $p = 9$ MPa (b) $p = 12$ MPa

(c) $p = 15$ MPa (d) $p = 18$ MPa

Figure 9: The distribution of plastic zone under various spherical stresses.

4.3. The Deformation Law of the Surrounding Rocks. The deformation of the roadway surrounding rocks under various spherical stresses is demonstrated in Figure 11.

According to Figure 11, (1) a threshold depth has been observed in rating the impact of spherical stress on the roadway surrounding rocks. When the spherical stress is higher than the threshold depth, the deformation is limited with a low degree of dispersion associated with the surrounding rock deformation. When the spherical stress is lower than the threshold depth, the deformation is severe with a high degree of dispersion associated with the surrounding rock deformation. (2) Under low spherical stress, the convergences in the deep and shallow surrounding rocks of roadway are negative and positive, respectively. As the spherical stress increases, the convergences from the deep to the shallow surrounding rocks become positive, suggesting that the increase of the spherical stress can lower the probability of the stratum separation. (3) As the spherical stress increases, the convergence value of the roadway surface surrounding rocks follows a linear growth.

4.4. The Distribution Law of the Third Invariant of Deviatoric Stress in Surrounding Rocks. A cloud shown in 12 was developed to demonstrate the distribution of the third invariant of deviatoric stress in the roadway surrounding rocks under various spherical stresses.

According to Figure 12, when $p = 9$ MPa, the roadway surrounding rocks are under pressure as a whole. When $p = 12$ MPa, a tensile stress zone was spotted around the roadway shallow rocks. As the spherical stress increased, multiple tensile stress zones were observed in the roadway sides and surrounding rocks of the roof. In other words, as the spherical stress increases, the tensile stress zone expands in the roadway surrounding rocks, reducing the loading capacity of the surrounding rocks. Therefore, in a high spherical stress environment, a high pretorque value should be adopted to the supporting system of the roadway surrounding rocks to enhance the load capacity of the surrounding rocks in roadway.

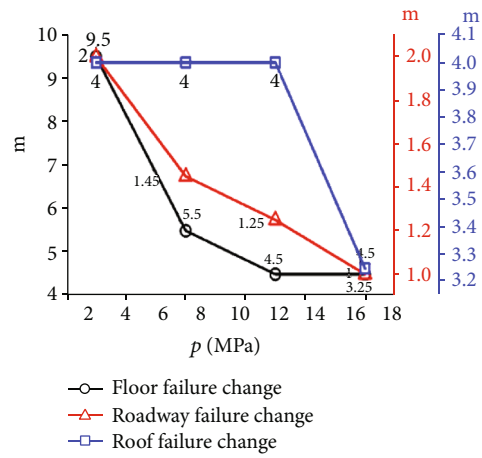

Figure 10: The damage depth of the surrounding rocks corresponding to the spherical stress.

5. The Instability Analysis of the Roadway Surrounding Rocks

5.1. The Analysis of the Impact of Deviatoric Stress on the Instability of the Roadway Surrounding Rocks. Taking equation (2) into consideration, the actual deviatoric stress of the roadway surrounding rocks depends on the ratio of three principal stresses instead of the individual value of three principal stresses, which is known as the lateral pressure coefficient. In other words, the deviatoric stress of the roadway surrounding rocks in a deep roadway under high ground stress does not necessarily lead to high deviatoric

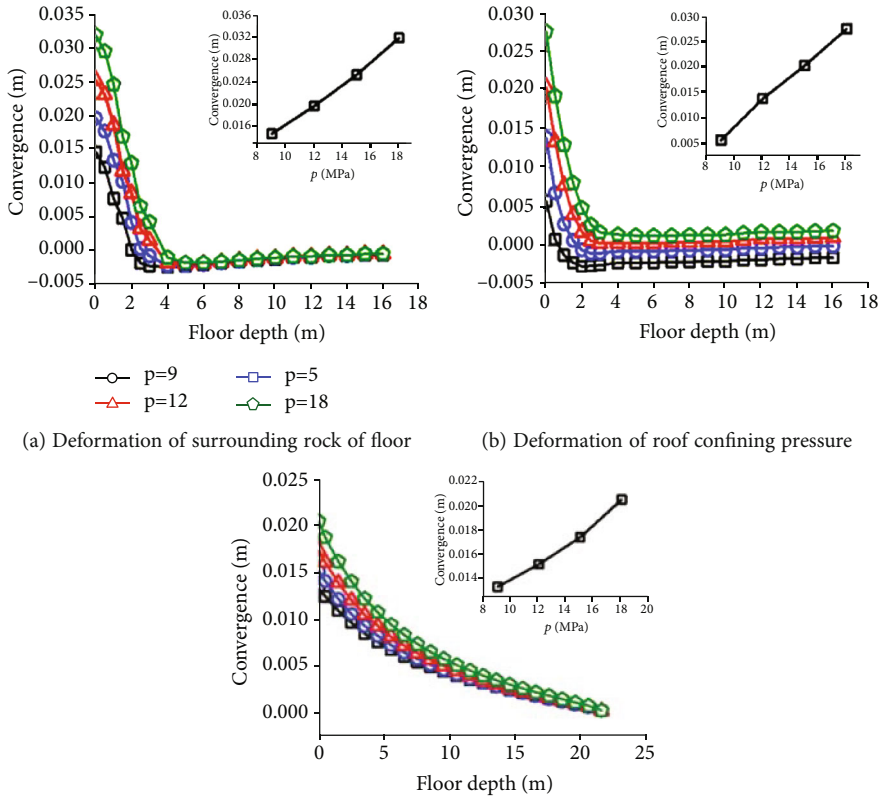

(a) Deformation of surrounding rock of floor

(b) Deformation of roof confining pressure

(c) Deformation of surrounding rock of roadside

Figure 11: The convergence of roadway surrounding rock under various spherical stresses.

stress. The deviatoric stress of the roadway surrounding rocks in a shallow roadway under high ground stress does not necessarily lead to low deviatoric stress either. According to the analysis in Section 3, the deviatoric stress tends to play a critical role in influencing the stability of the roadway surrounding rocks. In fields, many shallow roadways under low stresses tend to experience roof collapse and ground drums, such as the roadway located in the mines of the Shendong area. Therefore, according to the analysis in Section 3 along with the field investigation, some common misunderstandings have been identified to the support and protection system in the shallow surrounding rocks under low stress.

Firstly, according to Figures 4 and 5, the deviatoric stress tends to have a significant impact on the damage range and depth of the roadway surrounding rocks. However, regarding the shallow roadway under high deviatoric stress, the impacts of the stress on the stability of the roadway surrounding rocks are often overlooked during the design of the support and protection system, assuming that due to the shallow location of the roadway, no additional support system is needed, leading to a design of support and protection system shown in Figure 13.

As a result, the support and protection system lacks solid anchor points, accompanied by anchor bolts and cables following the movements of the surrounding rocks.

According to Figure 6 and the analysis in Section 3.3, as the deviatoric stress increases, the convergence of the roadway surrounding rocks increases accordingly, along with potential separation in the roadway roof. Without a strong support system such as a low elongation in anchor bolts and cables, a low support density, and a low strength in the metal protection net, the protection system could risk a total failure, resulting in severe deformation in the roadway sides including roof collapse and floor drums.

According to Figure 7, as the deviatoric stress increases, the tensile deformation continues to expand in the roadway surrounding rocks. Due to the poor tensile strength of the rocks, the expansion of the tensile deformation contributes to the increasing of the plastic zone and decreasing of the roadway stability, which is also reflected in Figure 4. With a low rigid support and protection system, such as a low pretorque value and poor timing for the installation of the support and protection system, a large tensile deformation zone can occur in the surrounding rocks, resulting in the continuous expansion of the plastic zone and severe deformation to the surrounding rocks in a high deviatoric stress environment.

5.2. The Analysis of the Impact of Spherical Stress on the Instability of the Roadway Surrounding Rocks. According to equation (1), the spherical stress value mainly depends on three principal stresses. It is commonly known that a greater depth leads to higher spherical stress. Based on Section 4, the spherical stress exerts a significant impact on the damage range of the roadway surrounding rocks, bearing capacity, and the deformation of the surrounding rocks.

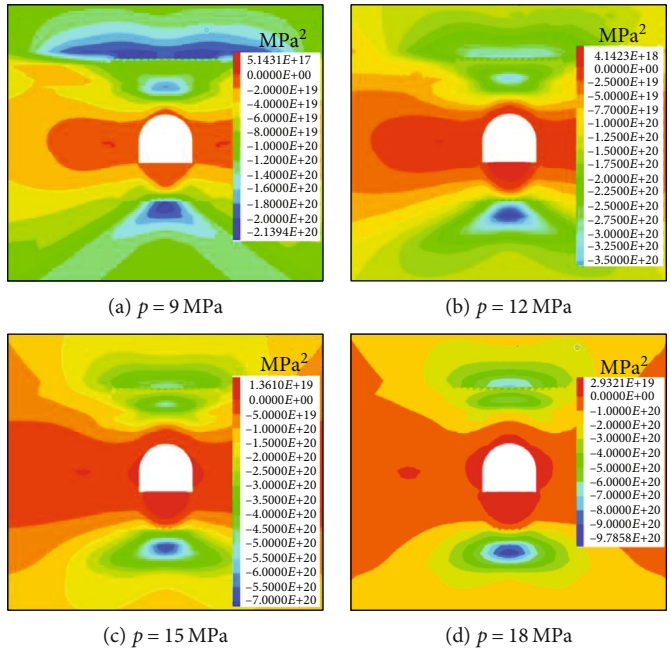

(a) $p = 9$ MPa (b) $p = 12$ MPa

(c) $p = 15$ MPa (d) $p = 18$ MPa

Figure 12: The J_3 distribution under various spherical stresses.

Therefore, according to the analysis in Section 4 and Figure 14 along with the field investigation, some common misunderstandings have been identified to the support and protection system in the shallow surrounding rocks under low stress including increasing the supported depth of the anchor bolts and cables blindingly and lacking specificity in the design of the support system.

In the fields, engineers and designers are misled to believe that a deeper roadway tends to experience more severe damage, resulting in increasing the supported depth blindingly. Based on the analysis in Sections 3 and 4, the damage range of the roadway surrounding rocks increases along with the increase of deviatoric stress and decrease of the spherical stress. As a result, regarding a roadway in an environment featured with high spherical stress and low deviatoric stress, the damage of the surrounding rocks should be limited, eliminating the need of increasing the supported depth. However, the increase of spherical stress tends to lead to the increase in the deformation of the roadway surrounding rocks, principal stress difference, and tensile stress zone, demanding a support system featured with high strength, shear resistance, and contractibility. Therefore, for the deep roadway in an environment featured with high spherical stress and low deviatoric stress, the support system should be improved by increasing the strength, shear resistance, and contractibility instead of the supported depth.

Due to insufficient theoretic guidance, the understandings of the critical factors of the stability of roadway surrounding rocks are limited. For instance, as demonstrated in Figure 9, the damage of the surrounding rocks concentrated in the roadway shoulders and bottom corners instead of the roadway sides. Therefore, the roadway shoulders and bottom corners should be the main protection targets.

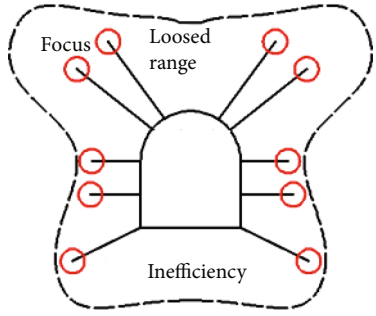

Figure 13: Misled roadway support system under a high deviatoric stress.

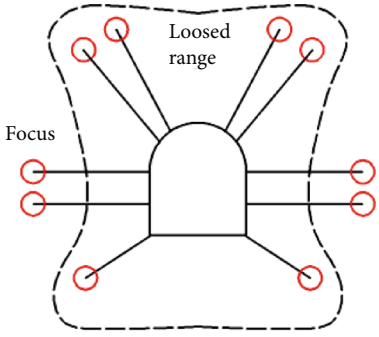

Figure 14: The roadway support misunderstanding under a high spherical stress.

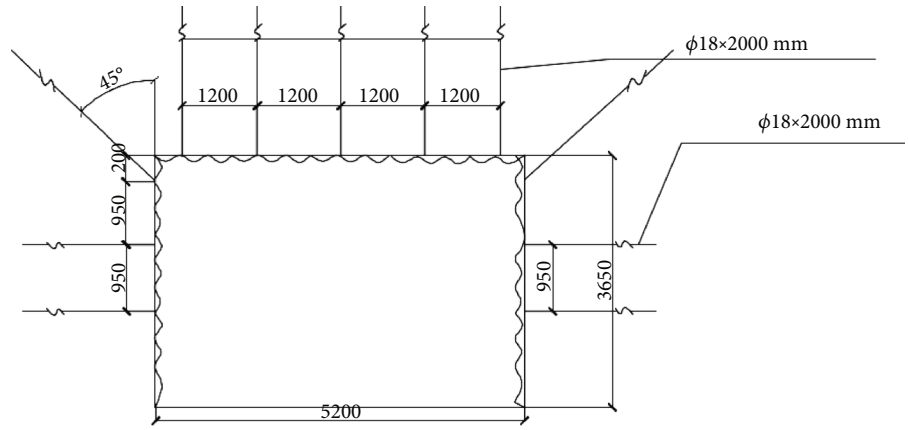

Figure 15: Original supporting plan.

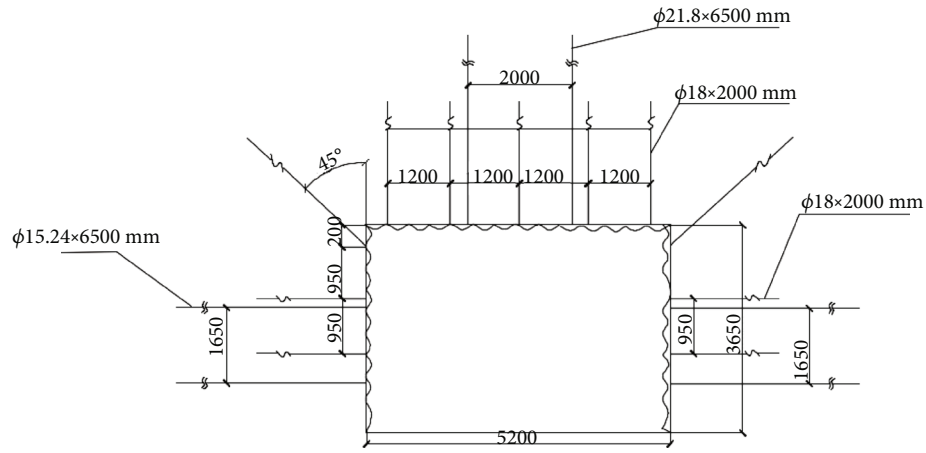

Figure 16: Modified support plan.

6. Engineering Validation

6.1. Project Overview and Maintenance Measures. A mine located in Inner Mongolia was selected for the purpose of engineering validation. The mining focuses on the #3 coal seam with an average thickness of 5 m, categorized as a horizontal coal seam with an average depth of 275 m. Currently, 310 working face is about 300 m away from the stopping mining line. No. 311 working face is featured with a through open cut. The transportation roadway of the No. 311 working face is 230 m away from the No. 310 goaf. Therefore, the No. 311 transportation roadway is not influenced by the mining process. Due to the depth of the #3 coal seam, the limited ground force, and relatively simple geological structure, supports were only added to the transportation roadway roof and sides, as demonstrated in Figure 15. The support system includes steel anchor rods in Φ18mm × 2000 mm, arranged in a triangular layout with a row distance of 1200 mm × 1100 mm. Roadway sides were protected with steel anchor rods in Φ18mm × 2000 mm, arranged in a flower layout with a row distance of 950 mm × 1100 mm.

After the installation of the support system demonstrated in Figure 15, severe damage was spotted in the roof of the No. 311 transport roadway and roadway sides, with some anchor rod failures, such as migrating with the surrounding rocks, tears in the metal net, and more. Several deep damages concentrated on the roof along with maximum deformation of 200 mm in the bottom, risking roof collapse.

Considering the limited ground force at the location of No. 311 transport roadway and no influence from the mining process, No. 311 transport roadway damage was mainly caused by high deviatoric stress. Following the analysis in Section 3, the deformation of roadway surrounding rocks in a high deviatoric stress field is featured with large damage scale, large roadway surface displacement, potential stratum displacement in the roof, and large tensile stress zone, which were consistent with the deformation of No. 311 transport roadway. In addition, some improper designs were identified in the support plan of No. 311 transport roadway. Therefore, based on the research results, some adjustments were made to the original design plan shown in Figure 16.

Anchor cables can link the load structure of the anchor rods to the deep surrounding rocks, resulting in an interconnected and overlapped network structure in the effective stress zone, resulting in decreasing the tensile stress zone of the surrounding rocks and increasing the stability of the load-bearing structure [24]. Following this concept, the support design of the No. 311 transport roadway was modified as follows. In order to minimize the separation in the roof surrounding rocks and reduce the tensile zone, two additional high-strength and high-elongation prestressed steel strands (dimension of Φ21.8 mm × 6500 mm) were added with a preload no less than120 kN. The distance between two strands was designed at 2000 mm × 3300 mm. Meanwhile, in order to control the roadway deformation and tensile deformation and improve the support efficiency of the anchor rods, two additional high-strength prestressed steel strands were added with a row distance of 1650 mm × 3300 mm. Besides, an inclined anchor rod was installed at the roadway sides, 15° in contrast with the horizontal direction for the purpose of improving the stability of roadway bottom corners.

6.2. The Analysis of the Modified Support System. Multiple monitoring and detection points were set up to keep track of the roadway surface displacements. The collected data indicated that with the modified support system, the deformation rate of the surrounding rocks was initially maintained at 8~20 mm/d with a higher deformation rate identified in the roadway sides and roof. A total of 4 changes were observed to the roadway sides and roof. The deformation rate demonstrated a downward trend. At day 37, the deformation reached stability, indicating an effective support and protection to the transport roadway.

7. Conclusion

For the principal stress difference distribution of the circular roadway surrounding rocks under various spherical stresses and deviatoric stresses via theoretical analysis, the calculation results were consistent with the numerical simulation.

(1) Under constant spherical stress, the plastic zone, the probability of stratum separation of the roof, the convergence of the surrounding rocks, and the tensile zone increase along with the deviatoric stress. The principal stress difference of the surrounding rocks and the concentration zone of the maximum principal stress difference tends to increase as the deviatoric stress increases

(2) Under constant deviatoric stress, as the spherical stress increases, the plastic zone decreases while the convergence of the surrounding rocks and the tensile zone increases. In addition, higher spherical stress increases the principal stress difference of the surrounding rocks. Meanwhile, the concentration zone of the maximum principal stress difference tends to decrease as the spherical stress increases

(3) Some common misunderstandings about the roadway support in a high spherical stress field and in a high deviatoric stress field were proposed, which was further validated in the field. The field test suggests that the modified support system following the research results can achieve effective protection and support

Data Availability

The data used to support the findings of this study are included within the article.

Conflicts of Interest

The authors declare that they have no conflicts of interest.

Acknowledgments

This research was financially supported by the central government guides local science and technology development fund projects (216Z5401G), Guizhou Province High-Level Innovative Talent Training Program Funding Project ([2019]5675), and Scientific Research Projects of Higher Education Institutions in Hebei Province (Z2020124).

References

[1] M. C. He, H. P. Xie, S. P. Peng, and Y. D. Jiang, "Study on mechanics in deep mining engineering," *Chinese Journal of Rock Mechanics and Engineering*, vol. 24, no. 16, pp. 2803–2813, 2005.

[2] G. Wang, Y. Guo, P. Wang et al., "A new experimental apparatus for sudden unloading of gas-bearing coal," *Bulletin of Engineering Geology and the Environment*, vol. 79, no. 2, pp. 857–868, 2020.

[3] Z. J. Wen, E. R. Xing, S. S. Shi, and Y. Jiang, "Overlying strata structural modeling and support applicability analysis for large mining-height stopes," *Journal of Loss Prevention in the Process Industries*, vol. 57, pp. 94–100, 2019.

[4] K. Wang, Y. Guo, H. Xu, H. Dong, F. Du, and Q. Huang, "Deformation and permeability evolution of coal during axial stress cyclic loading and unloading: an experimental study," *Geomechanics and Engineering*, vol. 24, no. 6, pp. 519–529, 2021.

[5] J. Chen, W. M. Cheng, G. Wang, H. Li, and Y. Li, "New method of monitoring the transmission range of coal seam water injection and correcting the monitoring results," *Measurement*, vol. 177, p. 109334, 2021.

[6] J. Chen, W. M. Cheng, and G. Wang, "Simulation of the meso-macro-scale fracture network development law of coal water injection based on a SEM reconstruction fracture COHESIVE model," *Fuel*, vol. 287, p. 119475, 2021.

[7] X. X. Yang, H. W. Jing, K. F. Chen, and W. L. Wang, "Study on influence law of in-situ stress in deep underground rocks on the size of failure zone in roadway," *Journal of Mining & Safety Engineering*, vol. 30, no. 4, pp. 495–500, 2013.

[8] Y. F. Sun, "Affects of insitu horizontal stress on stability of surrounding rock roadway," *Journal of China Coal Society*, vol. 35, no. 6, pp. 891–895, 2010.

[9] P. F. Gou, Z. P. Zhang, and S. J. Wei, "Physical simulation test of damage character of surrounding rock under different levels of the horizontal stress," *Journal of China Coal Society*, vol. 34, no. 10, pp. 1328–1332, 2009.

[10] C. Zhu, M. C. He, M. Karakus, X. Cui, and Z. Tao, "Investigating toppling failure mechanism of anti-dip layered slope due to excavation by physical modelling," *Rock Mechanics and Rock Engineering*, vol. 53, no. 11, pp. 5029–5050, 2020.

[11] F. L. He and G. C. Zhang, "Stability analysis and control of deepunderground roadway subjected to high horizontal tectonic stress," *Journal of China University of Mining & Technology*, vol. 44, no. 3, pp. 466–476, 2015.

[12] X. M. Chen, *Elastoplastic Mechanics*, Science Press, Beijing, 2007.

[13] N. J. Ma, J. Li, and Z. Q. Zhao, "Distribution of the deviatoric stress field and plastic zone in circular roadway surrounding rock," *Journal of China University of Mining & Technology*, vol. 44, no. 2, pp. 206–213, 2015.

[14] W. J. Yu, G. H. Wu, C. Yuan, P. Wang, and S. H. Shao, "Failure characteristics and engineering stability control of roadway," *Journal of China Coal Society*, vol. 42, no. 6, pp. 1408–1419, 2017.

[15] S. R. Xie, S. H. Yue, and D. D. Chen, "Deviatoric stress evolution laws and control of surrounding rock at gob-sideentry retaining in deep backfilling mining," *Journal of China Coal Society*, vol. 43, no. 7, pp. 1837–1846, 2018.

[16] F. L. He and G. C. Zhang, "Stablity analysis and control of deep underground roadways subjected to high horizontal tectonic stress," *Journal of China University of Mining & Technology*, vol. 44, no. 3, pp. 466–476, 2015.

[17] L. Xu, H. K. Wu, B. Li, and T. Q. Xiao, "Stability and control of surrounding rock in ultra-high roadway," *Chinese Journal of Rock Mechanics and Engineering*, vol. 33, no. S2, pp. 3891–3902, 2014.

[18] K. J. Luo, H. L. Dong, and Q. C. Gao, "Deformation division for surrounding rock of circular roadway by considering rheology and the intermediate principal stress," *Journal of China Coal Society*, vol. 42, no. S2, pp. 331–337, 2017.

[19] X. B. Zhang, G. M. Zhao, and X. R. Meng, "Elastoplastic analysis of surrounding rock on circular roadway based on druckerprager yield criterion," *Journal of China Coal Society*, vol. 38, no. S1, pp. 30–37, 2013.

[20] L. Chen, X. B. Mao, M. Li, and Y. L. Chen, "Elastoplastic analysis of cracked surrounding rock in deep roadway based on druckerprager criterion," *Journal of China Coal Society*, vol. 42, no. 2, pp. 484–491, 2017.

[21] Z. J. Wen, S. L. Jing, Y. J. Jiang et al., "Study of the fracture law of overlying strata under water based on the flow- stress-damage model," *Geofluids*, vol. 2019, Article ID 3161852, 12 pages, 2019.

[22] G. T. Yang, *Introduction to Elastoplastic Mechanics*, Tsinghua University Press, Beijing, 2004.

[23] X. Wang, Z. J. Wen, Y. J. Jiang, and H. Huang, "Experimental study on mechanical and acoustic emission characteristics of rock-like material under non-uniformly distributed loads," *Rock Mechanics and Rock Engineering*, vol. 51, no. 3, pp. 729–745, 2018.

[24] F. L. He, X. M. Wang, L. Xu, H. K. Wu, and J. Wang, "Principal stress difference transfer law and support in large-section open-off cut," *Rockand Soil Mechanics*, vol. 35, no. 6, pp. 1703–1710, 2014.